Temporal coherence of the acoustic field forward propagated through a continental shelf with random internal waves

Zheng Gong[a)]
Department of Mechanical Engineering, Massachusetts Institute of Technology, Cambridge, Massachusetts 02139

Tianrun Chen
Department of Earth Atmospheric and Planetary Science, Massachusetts Institute of Technology, Cambridge, Massachusetts 02139

Purnima Ratilal
Department of Electrical and Computer Engineering, Northeastern University, Boston, Massachusetts 02115

Nicholas C. Makris
Department of Mechanical Engineering, Massachusetts Institute of Technology, Cambridge, Massachusetts 02139

(Received 25 April 2013; revised 13 August 2013; accepted 17 September 2013)

An analytical model derived from normal mode theory for the accumulated effects of range-dependent multiple forward scattering is applied to estimate the temporal coherence of the acoustic field forward propagated through a continental-shelf waveguide containing random three-dimensional internal waves. The modeled coherence time scale of narrow band low-frequency acoustic field fluctuations after propagating through a continental-shelf waveguide is shown to decay with a power-law of range to the $-1/2$ beyond roughly 1 km, decrease with increasing internal wave energy, to be consistent with measured acoustic coherence time scales. The model should provide a useful prediction of the acoustic coherence time scale as a function of internal wave energy in continental-shelf environments. The acoustic coherence time scale is an important parameter in remote sensing applications because it determines (i) the time window within which standard coherent processing such as matched filtering may be conducted, and (ii) the number of *statistically independent* fluctuations in a given measurement period that determines the variance reduction possible by stationary averaging.
 [http://dx.doi.org/10.1121/1.4824157]

PACS number(s): 43.30.Re [TDF] Pages: 3476–3485

I. INTRODUCTION

During acoustic propagation through a continental shelf waveguide, random compressibility and density fluctuations induced by the internal waves can cause significant acoustic field fluctuations and temporal coherence degradation.[1–7] The acoustic coherence time scale is an important parameter in remote sensing applications because it determines (i) the time window within which standard coherent processing, such as matched filtering, beamforming, and synthetic aperture processing may be conducted, and (ii) the number of *statistically independent* fluctuations in a given measurement period that determines the variance reduction possible by stationary averaging.[8,9] To model and characterize acoustic field fluctuations, earlier work in the 1970s and 1980s focused on ray theory to estimate temporal coherence by accumulating random phase fluctuations along isolated water-borne ray paths in the deep ocean.[2,10] Isolated water-borne ray paths, however, are typically not available in continental shelf environments, making it necessary to consider other approaches. Later work used two-dimensional (2D) Monte-Carlo simulations[11] and a normal mode based analytical model[12] to obtain temporal coherence functions in deep-ocean environments, but have not yet been applied to continental shelf waveguides.

Here, an analytical model[12–14] derived from normal mode theory is adapted and applied to estimate the temporal coherence of the acoustic field forward propagated through three-dimensional (3D) random internal waves in an otherwise range-independent continental shelf waveguide. The model includes the accumulated effects of multiple forward scattering through range-dependent random internal wave inhomogeneities and accounts for mode coupling as a result of the random scattering process in the first two moments of the acoustic field. Modeled acoustic coherence time scales are shown to decrease with increasing internal wave energy, to be consistent with those measured in several recent continental shelf transmission experiments,[15–20] and to follow a $-1/2$ power-law dependence on range beyond moderate propagation ranges ($\gg$1 km). The power law dependencies are consistent with those empirically determined by Yang[18] who showed the acoustic temporal coherence in various continental shelf environments follows a $-1/2$ power-law dependence on range for low- to mid-frequency signals (200 Hz to 3.5 kHz) propagating from 5 to 42 km in range for various internal wave energies.[15–17] The $-1/2$ power-law dependence on range is also consistent with both measured data[18,21–27] and ray theory analysis[28–30] for

[a)]Author to whom correspondence should be addressed. Electronic mail: zgong@mit.edu

 0001-4966/2013/134(5)/3476/10/$30.00

low- to mid-frequency signals in deep ocean waveguides beyond roughly 10 km range.

It is useful to briefly review the physics, methods, and fundamental assumptions used here. Following a differential marching procedure analogous to that used by Rayleigh in free space optics,[31] Ratilal and Makris[13] derived the first two statistical moments of the acoustic field forward propagated through a horizontally stratified ocean waveguide with 3D random inhomogeneities that included the accumulated effects of multiple forward scattering. The derivation is based upon a modal formulation[32,33] for coherent 3D scattering in an ocean waveguide, and the waveguide extinction theorem,[34] both of which stem directly from Green's theorem. The modal formulation adapted here was first developed by Ingenito[32] for harmonic scattering from a single object in an isovelocity stratified medium and later generalized by Makris and Ratilal[33] for coherent 3D scattering from both stochastic and deterministic scatterers in a horizontally stratified ocean waveguide.

Following Rayleigh's work on forward propagation in free space with random inhomogeneities, or the red sunset problem,[31] Raitlal and Makris[13] showed that the mean forward field in an ocean waveguide can be analytically marched through successive range slabs of inhomogeneities to include multiple forward scattering when (1) the field scattered from inhomogeneities within any single horizontal range slab is small compared to the incident field; (2) the thickness of any horizontal range slab of inhomogeneities is sufficiently small for the single scatter approximation to be valid within it and sufficiently large for modal decoupling to occur in the mean forward field; and (3) the medium's 3D inhomogeneities obey a stationary random process within the horizontal range slab and local Fresnel width in cross-range, but need not be stationary in the vertical or across successive range slabs. Forward scattering is dominated by contributions from within the cross-range Fresnel width between source to receiver, as determined analytically by stationary phase analysis similar to that used by Rayleigh[31] and Van der Hulst[35] in free space optics. The resulting mean forward field takes the form of a product of the incident field and an exponential factor with a complex phase that accumulate horizontal wavenumber change due to scattering from source to receiver [Eq. (83) of Ref. 13]. These horizontal wavenumber changes account for dispersion and attenuation caused by scattering through the inhomogeneities, through their real and imaginary parts, respectively [Eqs. (60a) of Ref. 13, (37) of Ref. 12, and (36) of Ref. 14]. The horizontal wavenumber changes are determined by the medium's expected scatter function density, which may vary as a function of range, depth, and azimuth to account for range, cross-range, and depth-dependent variations in the random inhomogeneities.

Ratilal and Makris[13] used a similar marching procedure to derive the mean power and second moment of the forward acoustic field [Eqs. (86) and (85) of Ref. 13]. The incremental change in acoustic power due to a single range slab of inhomogeneities can be expressed in terms of the depth integral of the second moment of the scattered field, as well as cross terms between the incident and scattered fields. This change can then be expressed as the product of the incident power, the difference between modal field variance and attenuation coefficients, and slab thickness. The acoustic power at the receiver range is then obtained by marching the incremental power change from source to receiver through direct integration. This power is expressed as a product of the incident power and an exponential factor that involves range integration of the difference between modal variance and attenuation coefficients from source to receiver [Eq. (30) of Ref. 13], where the waveguide extinction theorem[34] is used for energy conservation. The expected inhomogeneities then may vary as a function of range and depth in this formulation. The second moment of the field is then obtained [Eqs. (37), (40), (41), and (48) of Ref. 13] when modes are statistically uncorrelated.

II. ANALYTICAL MODEL FOR TEMPORAL COHERENCE OF THE ACOUSTIC POWER AND FIELD FORWARD PROPAGATED THROUGH TIME-VARYING 3D RANDOM INTERNAL WAVES IN A CONTINENTAL SHELF WAVEGUIDE

In this section, analytical expressions for the temporal correlation function of the acoustic power and field forward propagated through time-varying 3D random internal waves in a continental shelf waveguide are provided, following the derivation and marching procedure described in Refs. 12–14. Assumptions are made that (1) the random internal waves follow a stationary random process and (2) the medium in a single differential range slab is static over the time period the acoustic wave passes through it. This is a good approximation because the correlation time scale of medium fluctuation is much longer than the time it takes the acoustic wave to propagate through a single differential range slab. The assumption of modal independence is not required for the derivation of the temporal correlation function of the acoustic power,[13] but only used here to estimate the temporal correlation of the acoustic forward field at a specific receiver depth. It is approximately valid when the random component of the field becomes a circular complex Gaussian random variable,[8] since the independence of at least a few dominant modes is then necessary by the central limit theorem.

The origin of the coordinate system is placed at the air–water interface with the positive z axis pointing downward. The source is located at the horizontal origin $\mathbf{r_0} = (0, 0, z_0)$, while receiver coordinates are given by $\mathbf{r} = (x, y, z)$, and inhomogeneity centers are given by $\mathbf{r}_\chi = (x_\chi, y_\chi, z_\chi)$. Spatial cylindrical (ρ, ϕ, z) and spherical systems (r, θ, ϕ) are defined by $x = r \sin\theta \cos\phi$, $y = r \sin\theta \sin\phi$, $z = r \cos\theta$, and $\rho^2 = x^2 + y^2$. The horizontal and vertical wavenumber components for the nth mode in an isovelocity layer[32,36] are, respectively, $\xi_n = k \sin\alpha_n$ and $\gamma_n = k \cos\alpha_n$, where α_n is the elevation angle of the mode measured from the z axis. Here, $0 \le \alpha_n \le \pi/2$ so that the down- and up-going plane wave components of each mode have elevation angles α_n and $\pi - \alpha_n$, respectively. The corresponding vertical wavenumber of the down- and up-going components of the nth mode are γ_n and $-\gamma_n$, respectively, where $\Re\{\gamma_n\} \ge 0$. The azimuth angle of the mode is denoted by β. The wavenumber magnitude k equals the angular frequency ω divided by the sound speed c in the object layer, where $k^2 = \xi_n^2 + \gamma_n^2$. The geometry of spatial and wavenumber coordinates is shown in Fig. 1.

A. Temporal correlation function of the acoustic field forward propagated through a continental shelf waveguide

With the approximation that the medium in a single differential range slab is effectively static over the time period the acoustic wave passes through the slab, the temporal correlation function of the acoustic field forward propagated through a continental shelf waveguide in the presence of 3D random internal wave inhomogeneities, assuming statistical independence between acoustic modes, at a single receiver $\mathbf{r}$ can be expressed as

$$\begin{aligned}
\mathrm{Corr}_{\Psi\Psi^*}(\mathbf{r}|\mathbf{r_0},f,\tau) &= \langle \Psi_T(\mathbf{r}|\mathbf{r_0},f,t)\Psi_T^*(\mathbf{r}|\mathbf{r_0},f,t')\rangle \\
&= \mathrm{Cov}\Big(\Psi_T(\mathbf{r}|\mathbf{r_0},f,t),\Psi_T(\mathbf{r}|\mathbf{r_0},f,t')\Big) + \langle \Psi_T(\mathbf{r}|\mathbf{r_0},f,t)\rangle\langle \Psi_T^*(\mathbf{r}|\mathbf{r_0},f,t')\rangle \\
&= \sum_{n=1}^{M_{\max}} \frac{2\pi}{d^2(z_0)}\frac{1}{|\xi_n|\rho}|u_n(z_0)|^2|u_n(z)|^2 \mathrm{e}^{-2\Im\{\xi_n\rho+\int_0^\rho \nu_n(\rho_s)d\rho_s\}}\Big(\mathrm{e}^{\int_0^\rho \mu_n(\rho_s,\tau)d\rho_s}-1\Big) \\
&\quad +\sum_{n=1}^{M_{\max}}\sum_{m=1}^{M_{\max}} \frac{2\pi}{d^2(z_0)}\frac{1}{\sqrt{\xi_n\xi_m^*}\rho}u_n(z_0)u_m^*(z_0)u_n(z)u_m^*(z)\mathrm{e}^{i\Re\{(\xi_n-\xi_m)\rho+\int_0^\rho(\nu_n(\rho_s)-\nu_m(\rho_s))d\rho_s\}} \\
&\quad \times\ \mathrm{e}^{-\Im\{(\xi_n+\xi_m)\rho+\int_0^\rho(\nu_n(\rho_s)+\nu_m(\rho_s))d\rho_s\}},
\end{aligned} \tag{1}$$

following the derivation in Sec. IIIC of Ref. 13. Here Eq. (1) is similar to Eq. (85) of Ref. 13, but with $\mu_n(\rho_s,\tau)$ replacing $\mu_n(\rho_s)$, where $\mu_n(\rho_s,\tau)$ is referred to as the *temporal* variance coefficient which accounts for modal coupling and modal energy transferred from the mean field to the covariance field[12] and describes how the acoustic power and forward field decorrelate as time lag $\tau = t - t'$ increases. The total forward field is $\Psi_T(\mathbf{r}|\mathbf{r_0},f,t)$ at receiver $\mathbf{r}$ from a source at $\mathbf{r_0}$ after propagation through a random inhomogeneous continental shelf waveguide, where f is the acoustic frequency, t and t' are the times at receiver $\mathbf{r}$, ρ_s is the center of internal wave inhomogeneities, $d(z_0)$ and $u_n(z_0)$ are the density and amplitude of mode shape at source depth z_0, $u_n(z)$ is the amplitude of mode shape at receiver depth z, $M_{\max}$ is the mode number at which the modal summations can be truncated and still accurately represent the field, and $\nu_n(\rho_s)$ is the time independent horizontal wavenumber change of nth mode due to multiple forward scattering from internal wave inhomogeneities.[13] The modal horizontal wavenumber change $\nu_n(\rho_s)$ is complex, and it leads to both dispersion and attenuation in the mean forward field. The real part $\Re\{\nu_n(\rho_s)\}$, which accounts for modal dispersion, is given in Eq. (60a) of Ref. 13 as

$$\begin{aligned}
\Re\{\nu_n(\rho_s)\} = \int_0^\infty \frac{2\pi}{k}\frac{1}{\xi_n}\frac{1}{d(z_t)}\Bigg[&\Big(N_n^{(1)}\Big)^2 \\
&\times e^{i2\gamma_n z_t}\langle S_{\rho_s,z_\chi,t}(\pi-\alpha_n,\phi;\alpha_n,\phi)\rangle \\
&- N_n^{(2)}N_n^{(1)}\langle S_{\rho_s,z_\chi,t}(\alpha_n,\phi;\alpha_n,\phi)\rangle \\
&- N_n^{(1)}N_n^{(2)}\langle S_{\rho_s,z_\chi,t}(\pi-\alpha_n,\phi;\pi-\alpha_n,\phi)\rangle \\
&+ \Big(N_n^{(2)}\Big)^2 e^{-i2\gamma_n z_t}\langle S_{\rho_s,z_\chi,t}(\alpha_n,\phi;\pi-\alpha_n,\phi)\rangle\Bigg]dz_t,
\end{aligned} \tag{2}$$

where $\langle S_{\rho_s,z_\chi,t}(\alpha,\beta;\alpha_i,\beta_i)\rangle$ is the medium's expected scatter function density at (ρ_s,z_χ) and time t, ϕ is the azimuth of the receiver from the source, α_n is the previously defined modal elevation angle, and $N_n^{(1)}$ and $N_n^{(2)}$ are the amplitudes of down- and up-going modal plane waves for mode n in the layer centered at z_t. Assuming no power loss within the Fresnel region or in the forward direction for a 2D scattering process, the imaginary part $\Im\{\nu_n^{2-\mathrm{D}}(\rho_s)\}$, which accounts for the modal attenuation in the mean forward field, can be calculated from Eq. (37) of Ref. 12 as

$$\Im\{\nu_n^{2-\mathrm{D}}(\rho_s)\} = \frac{1}{2}\mu_n^{2-\mathrm{D}}(\rho_s,\tau=0), \tag{3}$$

where $\mu_n^{2-\mathrm{D}}(\rho_s,\tau)$ is defined in Eq. (5). For a 3D scattering process, out-of-plane scattering becomes important and leads to power loss in the forward direction. The imaginary part $\Im\{\nu_n^{3-\mathrm{D}}(\rho_s)\}$ can be calculated from Eq. (36) of Ref. 14 as

$$\begin{aligned}
\Im\{\nu_n^{3-\mathrm{D}}(\rho_s)\} = \frac{1}{4\pi}A_c(\rho_s,z_\chi,z_{\chi'})\sum_{m=1}^{\infty}\Re\Bigg\{&\frac{\xi_m^*}{|\xi_m|\Re\{\xi_n^*\}} \\
&\times\int_0^{2\pi}\langle|\Xi_h(m,n,\beta,0)|^2\rangle d\beta\Bigg\}
\end{aligned} \tag{4}$$

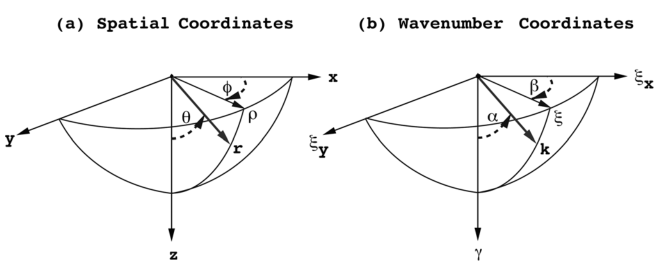

FIG. 1. The geometry of (a) spatial and (b) wavenumber coordinates.

by applying the waveguide extinction theorem,[34] where $\langle|\Xi_h(m,n,\beta,0)|^2\rangle$ is equivalent to $\Lambda(\rho_s,m,n,\tau)$ as defined in Eq. (7). As discussed in Sec. V B of Ref. 13, ν_n is independent of shell range ρ_s, so that $\int_0^\rho \nu_n(\rho_s)d\rho_s=\nu_n\rho$, where ρ is the horizontal source–receiver separation.

The *temporal* variance coefficient $\mu_n(\rho_s,\tau)$ depends on the relative size of the cross-range coherence length ℓ_y of the random internal wave inhomogeneities with respect to the Fresnel width[13] $Y_F(\rho,\rho_s)=\sqrt{\lambda(\rho-\rho_s)\rho_s/\rho}$ at a given shell range ρ_s, as discussed in Ref. 13. When $\ell_y>Y_F(\rho,\rho_s)$ or $|\rho_s-\rho/2|>(\rho/2)\sqrt{1-4\ell_y^2/(\lambda\rho)}$, scatterers are fully correlated across the active region or Fresnel width of the shell, which corresponds to an effective 2D scattering process for forward scatter. The *temporal* variance coefficient $\mu_n(\rho_s,\tau)$ can be expressed as

$$\mu_n^{2-\mathrm{D}}(\rho_s,\tau)=\sum_{m=1}^{M_{\max}}\frac{1}{|\xi_m|}\int_0^\infty \mathrm{d}z_\chi\int_0^\infty \mathrm{d}z_{\chi'}\frac{\ell_x(\rho_s,z_\chi,z_{\chi'})}{\xi_m}\times\frac{4\pi^2}{k(z_\chi)k(z_{\chi'})d(z_\chi)d(z_{\chi'})}\mathrm{C}_{s,s}(\rho_s,z_\chi,z_{\chi'},m,n,\tau),\tag{5}$$

which only depends on $\ell_x(\rho_s,z_\chi,z_{\chi'})$ for a 2D scattering process, where ℓ_x is the coherence length[13] of the internal wave inhomogeneities in the direction of acoustic propagation. When $\ell_y>Y_F(\rho,\rho/2)$ or $\rho<4\ell_y^2/\lambda$, the internal wave inhomogeneities are fully correlated in cross-range across the entire propagation path, so that from Eq. (91) of Ref. 13, we have

$$\int_0^\rho \mu_n(\rho_s,\tau)d\rho_s=\mu_n^{2-\mathrm{D}}(\rho_s,\tau)\,\rho=\sum_{m=1}^{M_{\max}}\frac{\rho}{\xi_m}\frac{\ell_x}{|\xi_m|}\Lambda(\rho_s,m,n,\tau),\tag{6}$$

where

$$\Lambda(\rho_s,m,n,\tau)=\int_0^\infty dz_\chi\int_0^\infty dz_{\chi'}\frac{4\pi^2}{k(z_\chi)k(z_{\chi'})d(z_\chi)d(z_{\chi'})}\times\mathrm{C}_{s,s}(\rho_s,z_\chi,z_{\chi'},m,n,\tau).\tag{7}$$

When $\ell_y<Y_F(\rho,\rho_s)$ within the shell at range ρ_s or $|\rho_s-\rho/2|<(\rho/2)\sqrt{1-4\ell_y^2/(\lambda\rho)}$, scatterers decorrelate in both range and cross-range within the Fresnel width of the shell, which leads to a 3D scattering process for forward scatter. The *temporal* variance coefficient $\mu_n(\rho_s,\tau)$ is given by

$$\begin{aligned}\mu_n^{3-\mathrm{D}}(\rho_s,\tau)&=\sum_{m=1}^{M_{\max}}\sqrt{\frac{\rho}{2\pi\xi_m\rho_s(\rho-\rho_s)}}\frac{1}{|\xi_m|}\times\int_0^\infty \mathrm{d}z_\chi\int_0^\infty dz_{\chi'}A_c(\rho_s,z_\chi,z_{\chi'})\\&\quad\times\frac{4\pi^2}{k(z_\chi)k(z_{\chi'})d(z_\chi)d(z_{\chi'})}\mathrm{C}_{s,s}(\rho_s,z_\chi,z_{\chi'},m,n,\tau)\\&=\sum_{m=1}^{M_{\max}}\sqrt{\frac{\rho}{2\pi\xi_m\rho_s(\rho-\rho_s)}}\frac{A_c}{|\xi_m|}\Lambda(\rho_s,m,n,\tau),\end{aligned}\tag{8}$$

which becomes a function of coherence area[13] $A_c(\rho_s,z_\chi,z_\chi')$ for a 3D scattering process. When $\ell_y<Y_F(\rho,\rho/2)$ or $\rho>4\ell_y^2/\lambda$, the internal wave inhomogeneities decorrelate in both range and cross-range only over the middle segment $(\rho_s^{\mathrm{cor}}<\rho_s<\rho-\rho_s^{\mathrm{cor}})$ of the propagation path, but are fully correlated at the beginning $(\rho_s<\rho_s^{\mathrm{cor}})$ or end $(\rho_s>\rho-\rho_s^{\mathrm{cor}})$, where $\rho_s^{\mathrm{cor}}=(\rho/2)\left(1-\sqrt{1-4\ell_y^2/(\lambda\rho)}\right)$. From Eqs. (88) and (90) of Ref. 13, we have

$$\begin{aligned}\int_0^\rho \mu_n(\rho_s,\tau)d\rho_s&=\int_0^{\rho_s^{\mathrm{cor}}}\mu_n^{2-\mathrm{D}}(\rho_s,\tau)d\rho_s+\int_{\rho_s^{\mathrm{cor}}}^{\rho-\rho_s^{\mathrm{cor}}}\mu_n^{3-\mathrm{D}}(\rho_s,\tau)d\rho_s+\int_{\rho-\rho_s^{\mathrm{cor}}}^{\rho}\mu_n^{2-\mathrm{D}}(\rho_s,\tau)d\rho_s\\&=\sum_{m=1}^{M_{\max}}2\left(\frac{\ell_x}{\xi_m}\rho_s^{\mathrm{cor}}+A_c\sqrt{\frac{\rho}{2\pi\xi_m}}\left[\sin^{-1}\sqrt{1-\frac{\rho_s^{\mathrm{cor}}}{\rho}}-\sin^{-1}\sqrt{\frac{\rho_s^{\mathrm{cor}}}{\rho}}\right]\right)\frac{1}{|\xi_m|}\Lambda(\rho_s,m,n,\tau).\end{aligned}\tag{9}$$

In Eqs. (5)–(9), $d(z_\chi)$ and $d(z_{\chi'})$ are the density at depth z_χ and $z_{\chi'}$ of internal wave inhomogeneities centered at ρ_s, respectively. They also contain a term

$$\mathrm{C}_{s,s}(\rho_s,z_\chi,z_{\chi'},m,n,\tau)=u_n(z_\chi)u_n^*(z_{\chi'})u_m(z_\chi)u_m^*(z_{\chi'})\times\mathrm{cov}_{ss}(\rho_s,z_\chi,z_{\chi'},\tau),\tag{10}$$

where $u_n(z_\chi)$, $u_n^*(z_{\chi'})$, $u_m(z_\chi)$, and $\mu_m^*(z_{\chi'})$ are the amplitude of the nth and mth mode shape at depth z_χ and $z_{\chi'}$ respectively, and $\mathrm{cov}_{ss}(\rho_s,z_\chi,z_{\chi'},\tau)\approx\langle s_{\rho_s,z_\chi,t}(\alpha,\beta;\alpha_i,\beta_i)s^*_{\rho_s,z_\chi,t'}(\alpha',\beta';\alpha'_i,\beta'_i)\rangle$ is the temporal covariance of the scatter function density [Eq. (34) of Ref. 12], which is also a linear function of the spatio-temporal covariance of internal wave displacements $\mathrm{cov}_{\xi\xi}(0,\tau,z_\chi,z_{\chi'})$, as can be seen from Eq. (35) of Ref. 12. In Eq. (31) of Ref. 12, it is shown that $\mathrm{cov}_{\xi\xi}(0,\tau,z_\chi,z_\chi')$ can be directly expressed as

$$\mathrm{cov}_{\xi\xi}(0,\tau,z_\chi,z_{\chi'})=\sum_{j=1}^{\infty}\int F_j(\boldsymbol{\sigma})W_j(\sigma,z_\chi)W^*(\sigma,z_{\chi'})\times\mathrm{e}^{-i\omega(\sigma,j)\tau}d^2\boldsymbol{\sigma},\tag{11}$$

where

$$F_j(\boldsymbol{\sigma}) = E(\mathcal{A})M(j^2 + j_*^2)^{-p/2}\left(\frac{4}{\pi}\right)\frac{k_j\sigma^2}{(\sigma^2 + k_j^2)^2} \tag{12}$$

is the G-M internal wave spectrum,[2] and $W_j(\sigma, z_\chi)$ is the jth modal shape of internal waves at depth z_χ. Here, $\boldsymbol{\sigma} = (\sigma_x, \sigma_y)$ is the internal wave wavenumber vector, (σ_x, σ_y) are the components of the wavenumber in the (x, y) directions, and $\sigma = (\sigma_x^2 + \sigma_y^2)^{1/2}$. The average energy density in Joule m^{-2} that determines the strength of the internal wave fluctuations is $E(\mathcal{A}) = \mathcal{A}E_0$, where E_0 is the average energy density of the internal wave, and $\mathcal{A}$ is a scaling factor for the G-M internal wave energy level. For example, for the 0.5 G-M internal wave energy level, $\mathcal{A} = 0.5$. As suggested by Tielburger *et al.*,[37] $E_0 = 25\,\mathrm{Jm}^{-2}$ was used in all examples shown in Sec. III to simulate 3D random internal wave inhomogeneities in a slowly time-varying continental shelf waveguide. This value is physically valid because it satisfies the displacement constraint which requires the displacement at any depth z must be within the waveguide boundaries.[37] The quantity k_j, which corresponds to the spectral peak in the horizontal wavenumber domain for each mode j, is given by $k_j = \pi j f_c / \int_0^H n(z_\chi)dz_\chi$, where $f_c = 2\Omega\sin(\text{latitude})$ is the Coriolis frequency, which is roughly 1.49×10^{-5} Hz at 40° latitude, H is the water-column depth of the waveguide, and $n(z_\chi)$ is the buoyancy frequency or *Brunt-Väisälä* frequency at depth z_χ. The normalization factor M satisfies $1/M = \sum_{j=1}^{\infty}(j^2 + j_*^2)^{-p/2}$. The characteristic mode number j_* and spectral power law exponent p are empirically determined, which control the relative contribution of the internal wave modes.[37] Here, for random internal wave inhomogeneities in continental shelf waveguides, we use $j_* = 1$ and $p = 4$, as suggested by Yang and Yoo,[38] instead of $j_* = 3$ and $p = 2$ from G-M model, which are empirically determined for the deep ocean environments.[2]

It is important to note that we assume the internal wave field within each horizontal range slab follows a stationary random process. The point then is not to determine specific spatial and temporal realizations of acoustic temporal coherence fluctuations resulting from specific spatial and temporal realizations of internal wave fields, but rather to determine the mean temporal coherence corresponding to internal wave fields that obey spatial and temporal random process that may have many realizations. Since the measured internal wave energies used in the present investigation were measured over roughly 12 h, the expectation values used here should be considered to represent mean values over a similar time period for each slab. Such mean statistics are valid for many specific realizations of spatial and temporal internal wave fields so long as the internal wave statistics are appropriate for each range slab and averaging time period, which is necessarily the case when the mean statistics are based on direct measurements as they are here.

B. Temporal correlation function for acoustic power of the forward field

The temporal correlation function of the acoustic power at receiver $\mathbf{r} = (\boldsymbol{\rho}, z)$ is the depth-integrated temporal correlation function of Eq. (1), which can be written as

$$\begin{aligned}\langle W_T(\boldsymbol{\rho}|\mathbf{r_0},\tau)\rangle &= \int_0^\infty \frac{1}{d(z)}\langle\Psi_T(\mathbf{r}|\mathbf{r_0},f,t)\Psi_T^*(\mathbf{r}|\mathbf{r_0},f,t')\rangle dz \\ &= \sum_{n=1}^{M_{\max}} W_i^{(n)}(\boldsymbol{\rho}|\mathbf{r_0})\mathrm{e}^{\int_0^\rho(\mu_n(\rho_s,\tau)-2\Im\{\nu_n(\rho_s)\})\mathrm{d}\rho_s},\end{aligned} \tag{13}$$

following the marching procedure described in Sec. III B of Ref. 13, where modal orthogonality,

$$\int_0^\infty \frac{1}{d(z)}u_m^*(z)u_n(z)dz = \delta_{nm} \tag{14}$$

collapses the double modal sum in the second term of Eq. (1) into a single sum and leads to cancellation with

$$\sum_{n=1}^{M_{\max}} \frac{2\pi}{d^2(z_0)}\frac{1}{|\xi_n|\rho}|u_n(z_0)|^2\mathrm{e}^{-2\Im\{\xi_n\rho+\int_0^\rho\nu_n(\rho_s)d\rho_s\}} \tag{15}$$

in the first term of Eq. (1). In Eq. (13),

$$W_i^{(n)}(\boldsymbol{\rho}|\mathbf{r_0}) = \frac{2\pi}{d^2(z_0)}|u_n(z_0)|^2\frac{1}{\rho|\xi_n|}\mathrm{e}^{-2\Im\{\xi_n\}\rho} \tag{16}$$

is the depth-integrated second moment of acoustic incident field of mode n in a static ocean waveguide when internal wave inhomogeneities are absent. In Sec. III, we apply Eqs. (1) and (13) to calculate the temporal correlation function of the acoustic field and power forward propagated through 3D random internal waves with different internal wave energy levels.

III. RESULTS AND DISCUSSION

A. Modeled continental shelf environments

A water column of 80 m depth is used to simulate the geometry of a continental shelf environment. The bottom sediment half-space is composed of sand with density $d_b = 1.9\,\mathrm{g/cm^3}$ and sound speed $c_b = 1700$ m/s. The attenuation coefficients in the water column and bottom are $\alpha = 6 \times 10^{-5}\,\mathrm{dB}/\lambda$ and $\alpha_b = 0.8\,\mathrm{dB}/\lambda$, respectively. A point source transmits monochromatic acoustic waves at a frequency of 415 Hz. Both the source and point receiver are located at a depth of 40 m. Source–receiver separations, ranging from 5 to 42 km, are used to simulate typical scenarios employed in three shallow water acoustic experiments:[15–17] (a) the SWARM95 experiment, conducted from July to August of 1995 in the Mid-Atlantic bight off the coast of New Jersey; (b) the ADVENT99 experiment, conducted from April to May of 1999 in the Strait of Sicily, Mediterranean; and (c) the ASCOT01 experiment, conducted in June of 2001 in the Gulf of Maine along the contour of 100 m depth. Here, a sound speed profile, downward refracting in the upper water column and roughly constant in the lower water column, which illustrates the fundamental physics of internal waves in two-layer mid-latitude continental shelf environments, is used for simulations, as shown in Fig. 2. The sound speed profile used here is calculated by averaging 100 *in situ* measurements of sound speed profiles

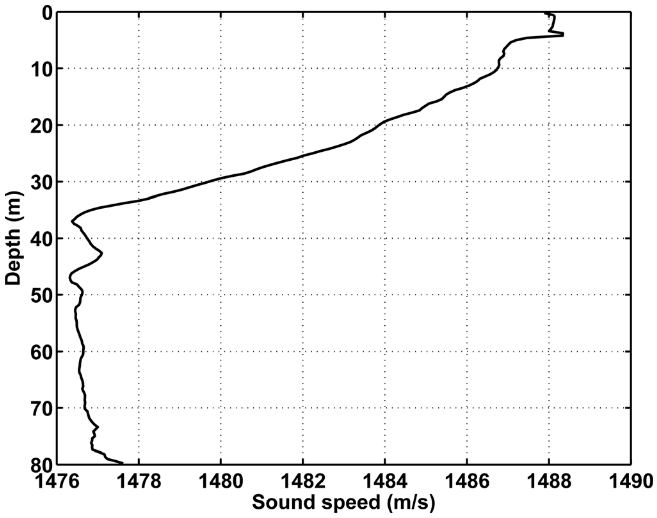

FIG. 2. Mean sound speed profile averaged over 100 *in situ* measured sound speed profiles made by both conductivity-temperature-depth (CTD) and expendable bathythermographs (XBTs) during May–June 2003 in New Jersey STRATAFORM.

made by both conductivity-temperature-depth (CTD) and expendable bathythermographs (XBTs) during May–June 2003 in New Jersey STRATAFORM.

Yang[18] empirically investigated the coherence time scale of acoustic signals in three typical two-layer mid-latitude continental shelf environments that have warm water near the sea surface and cooler water below.[16,17,39] He found that higher standard deviations of sound speed at the depth of the thermocline corresponded to higher internal wave energies and lower acoustic coherence time scales. In particular, he found increasing internal wave energies and decreasing coherence time scales for the ADVENT99, ASCOT01, and SWARM95 experiments, respectively. In this paper, we analytically investigate the coherence time scales of acoustic signals in mid-latitude two-layer continental shelf environments as a function of internal wave energy. Using similar low, medium and high internal wave energies as Yang, with all other parameters fixed as a control, we show that the modeled coherence time scales of acoustic signals decreases with increasing internal wave energy, consistent with the experimental findings of Yang.[18] If internal wave amplitude was held fixed, increasing the sound speed gradient at the thermocline would increase the buoyancy frequency and consequently internal wave energy, which would lead to a decrease in the coherence time scales of acoustic signals.

B. Illustrative examples by simulation

Temporal coherence of acoustic power $\varrho^{\text{power}}(\boldsymbol{\rho},\tau)$ at receiver $\mathbf{r}=(\boldsymbol{\rho}, z)$ is given by

$$\varrho^{\text{power}}(\boldsymbol{\rho},\tau) \equiv \frac{\langle W_T(\boldsymbol{\rho}|\mathbf{r_0},\tau)\rangle}{\langle W_T(\boldsymbol{\rho}|\mathbf{r_0},0)\rangle}, \quad (17)$$

where $\langle W_T(\boldsymbol{\rho}|\mathbf{r_0},\tau)\rangle$ is the temporal correlation function of acoustic power, as defined in Eq. (13). Temporal coherence of acoustic forward field $\varrho^{\text{field}}(\mathbf{r},\tau)$ at receiver $\mathbf{r}=(\boldsymbol{\rho}, z)$ is given by

$$\varrho^{\text{field}}(\mathbf{r},\tau) \equiv \frac{\langle \Psi_T(\mathbf{r}|\mathbf{r_0},f,t)\Psi_T^*(\mathbf{r}|\mathbf{r_0},f,t')\rangle}{\langle \Psi_T(\mathbf{r}|\mathbf{r_0},f,t)\Psi_T^*(\mathbf{r}|\mathbf{r_0},f,t)\rangle}, \quad (18)$$

where $\langle \Psi_T(\mathbf{r}|\mathbf{r_0},f,t)\Psi_T^*(\mathbf{r}|\mathbf{r_0},f,t')\rangle$ is the temporal correlation function of acoustic forward field, as defined in Eq. (1). Two criteria are employed to define the coherence time scale: (a) the e-folding coherence time scale τ_e; and (b) the $\tau_{0.8}$ coherence time scale, which corresponds to the time at which the temporal coherence $\varrho^{\text{power}}(\boldsymbol{\rho},\tau)$ or $\varrho^{\text{field}}(\mathbf{r},\tau)$ falls to $1/e$ and 0.8 of its zero time lag value, respectively, such that $\varrho^{\text{power}}(\boldsymbol{\rho},\tau_e)$ or $\varrho^{\text{field}}(\mathbf{r},\tau_e)=1/e$ and $\varrho^{\text{power}}(\boldsymbol{\rho},\tau_{0.8})$ or $\varrho^{\text{field}}(\mathbf{r},\tau_{0.8})=0.8$. The $\tau_{0.8}$ coherence time scale is used primarily for comparison with the measured temporal coherence reported by Yang.[18]

The modeled acoustic coherence time scales τ_e^a and $\tau_{0.8}^a$ are found to decrease with increasing internal wave energy, as shown in Fig. 3, where the temporal correlation function of the depth-averaged acoustic intensity and the acoustic forward field for acoustic signals propagating from 5 to 42 km in range are plotted as a function of time lag (min) for various internal wave energies following Eqs. (1) and (13), respectively. In the presence of weak internal waves ($\mathcal{A}=1/4$) and at shorter ranges (<10 km), the fluctuations in the temporal correlation function of the acoustic forward field, as shown in Fig. 3(b), are mainly due to the fluctuations in the squared mean field [second term of Eq. (1)] or coherent intensity due to modal interference.[14] This fluctuation becomes negligible beyond moderate propagation ranges (>10 km) or in the presence of strong internal waves because (1) the severe attenuation induced by internal wave scattering makes the squared mean field decaying rapidly with range; and (2) the field covariance [first term of Eq. (1)] or incoherent intensity begins to dominate the total field, which causes the acoustic forward field to become fully saturated and lose range- and depth-dependent coherent modal interference structure.[14]

Our modeled acoustic coherence time scales $\tau_{0.8}^a$ at three source–receiver separations, 5, 10, and 42 km, are shown to be of the same order of magnitude and to follow the same trend as a function of range with those experimentally determined $\tau_{0.8}^a$ for narrow band low-frequency acoustic signals during two shallow water experiments,[18] as can be seen from Fig. 4. This consistency gives added confidence to the veracity of our analytical model, which should provide a useful means of estimating or predicting acoustic coherence time scale.

Our model also shows that higher internal wave energy leads to larger decreases in acoustic coherence time scales at shorter ranges than at longer ranges, as shown in Fig. 4, as will be seen again in Sec. III C when the power-laws in range are described. For instance, the modeled τ_e^a shows an order of magnitude increase, from 4.0 to 50.0 min, when $\mathcal{A}$ decreases from 4 to 1/4 at 5 km source–receiver separation, while it only increases by five times (from 1.2 to 6.0 min) when the source–receiver separation increases to 42 km. This difference will be quantified later as a scaling factor of the power-law range dependence.

The internal wave e-folding τ_e^{iw} and $\tau_{0.8}^{iw}$ coherence time scales in a continental shelf environment are seen to be approximately 1 h and 16 min, respectively, for

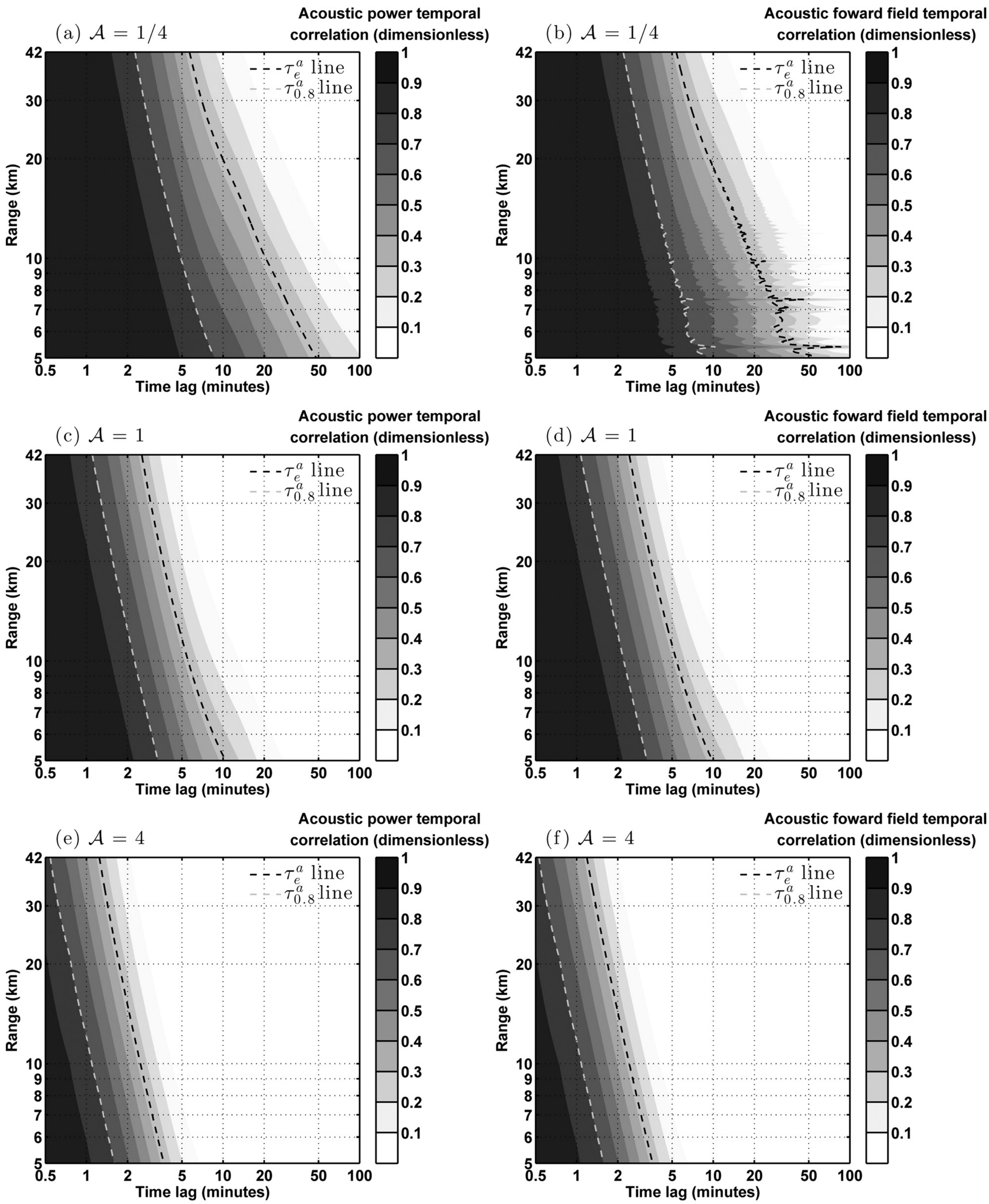

FIG. 3. (a)–(f) Two-dimensional (2D) temporal coherence of the acoustic power and forward field are plotted on logarithmic scales of time lag (min) and range (km) for three internal wave energies, $\mathcal{A} = 1/4$, 1, and 4. The source and receiver are both located at the middle of the water column (40 m) in a continental shelf waveguide of 80 m water depth. The temporal coherence of the acoustic power and forward field at a given range are given by Eqs. (17) and (18). The G-M internal wave energy is calculated using Eq. (12). The dashed black line (τ_e^a line) is plotted at the correlation function value $1/e$, and the dashed gray line ($\tau_{0.8}^a$ line) is plotted at the correlation function value 0.8.

displacements at the middle of the water column (40 m), as shown in Fig. 5 following Eq. (31) of Ref. 12. They are typically an order of magnitude larger than those of the acoustic forward field (Fig. 4). This is mainly due to *accumulated* multiple forward scattering, which causes dramatic degradation in the temporal coherence of the acoustic forward field as it propagates through internal wave inhomogeneities.

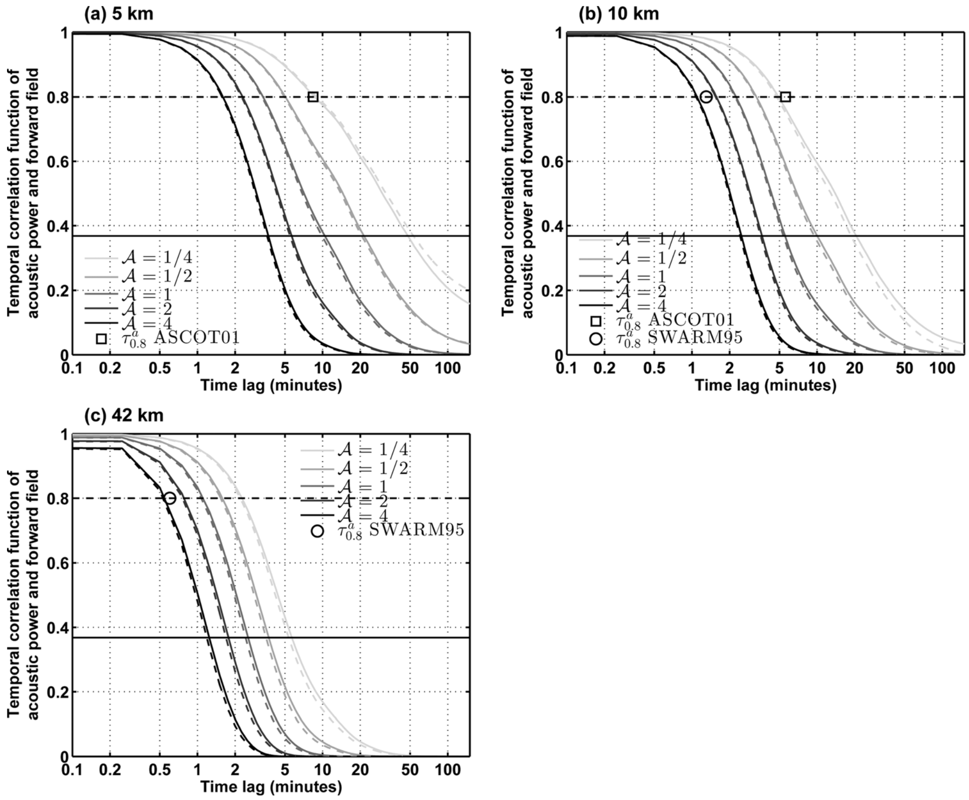

FIG. 4. Temporal coherence of acoustic power (solid lines) and forward field (dashed lines) in a continental shelf waveguide is plotted on a logarithmic scale of time lag for low-frequency acoustic signals propagating 5 km in range for five different internal wave energies ($A = 1/4$, $1/2$, 1, 2, and 4). The source and receiver are both located at the middle of the water column (40 m). The temporal coherence of the acoustic power and forward field are given by Eqs. (17) and (18). The G-M internal wave energy is calculated using Eq. (12). The solid black horizontal line is plotted at the correlation function value $1/e$, and the dashed black horizontal line is plotted at the correlation function value 0.8. (a) The modeled e-folding τ^a_e and $\tau^a_{0.8}$ coherence time scales of the acoustic signals propagating 5 km in range for five different internal wave energies. (b) Similar to (a) but for acoustic signals propagating 10 km in range. (c) Similar to (a) but for acoustic signals propagating 42 km in range. The experimentally determined mean $\tau^a_{0.8}$ of narrow band acoustic signals at three discrete source–receiver separations (5, 10, and 42 km) measured during the ASCOT01 experiment (black squares) and the SWARM95 experiment (black circles) are overlain.

C. Dependence of acoustic coherence time scales on range and internal wave energy in continental shelf environments

Given the modeled τ^a_e and $\tau^a_{0.8}$ for both the acoustic power and forward field, we investigate the dependence of the temporal coherence of low-frequency acoustic field on range and internal wave energy in typical two-layer mid-latitude continental shelf environments.

We show that both τ^a_e and $\tau^a_{0.8}$ of the acoustic power (solid lines in Fig. 6) and forward field (dashed lines in Fig. 6) follow a power-law of $\rho^{-1/2}$ (dashed-dotted black lines) beyond moderate propagation ranges ($\rho \gg 1$ km), as shown in Fig. 6. The power-law dependencies are found to be consistent with those empirically determined by Yang[18] who showed the acoustic temporal coherence in various continental shelf environments also follows a power-law of $\rho^{-1/2}$ for low- to mid-frequency signals propagating from 5 to 42 km in range for various internal wave energies.[15–17] The power-law of $\rho^{-1/2}$ is also consistent with both measured data[21–27] and ray theory analysis[28–30] for low- to mid-frequency signals in deep ocean waveguides beyond roughly 10 km range.

At short ranges, the modeled τ^a_e and $\tau^a_{0.8}$ of the acoustic forward field begin to fluctuate, as can be seen from Fig. 6 (dashed lines), depending on internal wave energy. The fluctuation is mainly because the assumption the temporal coherence of the acoustic forward field, becomes invalid at sufficiently short range or low internal wave energy. The mean trend in this regime, however, may likely still provide

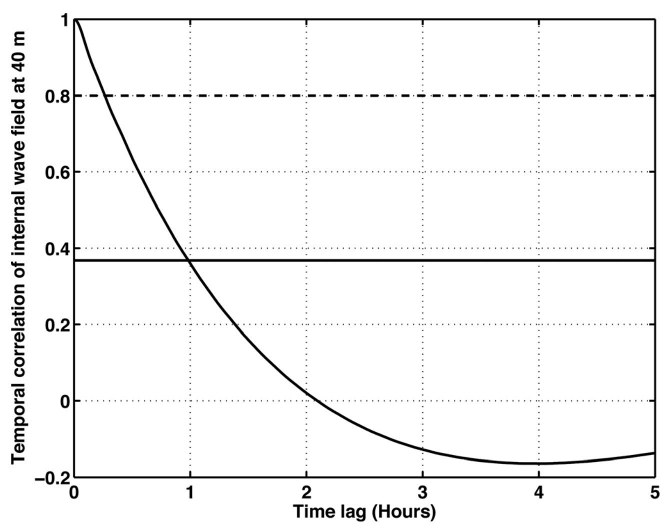

FIG. 5. Temporal coherence of internal wave displacement at 40 m depth as a function of time lag in a continental shelf environment of 80 m water depth. The temporal coherence is the *normalized* spatio-temporal covariance of Eq. (31) in Ref. 12. The internal wave e-folding τ^{iw}_e and $\tau^{iw}_{0.8}$ coherence time scales are approximately 1 h and 16 min, respectively. The solid black horizontal line is plotted at the correlation function value $1/e$, and the dashed black horizontal line is plotted at the correlation function value 0.8.

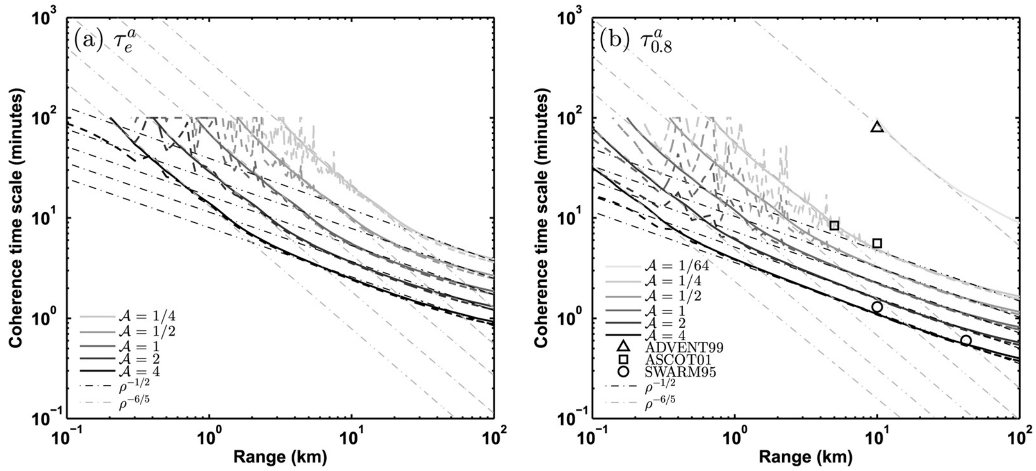

FIG. 6. Modeled e-folding τ_e^a and $\tau_{0.8}^a$ coherence time scales of low-frequency acoustic power (solid lines) and forward field (dashed lines) as a function of range for five different internal wave energies. The fluctuations in τ_e^a and $\tau_{0.8}^a$ of the acoustic forward field are mainly due to the fluctuations in the squared mean field or coherent intensity due to modal interference. The dashed-dotted gray lines and dashed-dotted black lines in (a) indicate the power-law of $\rho^{-6/5}$ and the power-law of $\rho^{-1/2}$ obtained from Eq. (19) that best fit our modeled τ_e^a, respectively. Similar line plots of the power-law range dependence are shown in (b) but for the best fit with our modeled $\tau_{0.8}^a$, obtained from Eq. (20). Black triangle, squares, and circles in (b) indicate the experimentally determined $\tau_{0.8}^a$ of narrow band acoustic signals centered at 415 Hz (i) at 10 km range in the Strait of Sicily, Mediterranean during the ADVENT99 experiment; (ii) at 5 and 10 km range in the Gulf of Maine during the ASCOT01 experiment; and (iii) at 10 and 42 km range in the New Jersey STRATAFORM during the SWARM95 experiment, respectively.

a reasonable approximation to the power-law since the temporal coherence for depth integrated intensity does not require a modal independence assumption. Interestingly, at such short ranges, the modeled τ_e^a and $\tau_{0.8}^a$ of the acoustic field (solid lines in Fig. 6) follow a power-law of $\rho^{-6/5}$ (dashed-dotted gray lines), which is similar to the power-law of $\rho^{-3/2}$ previously found for deep ocean environments by *ray theory*[28–30] for high-frequency signals (roughly $>$ 10 kHz) within 1 km range. Experimental measurements of coherence time scale at such short ranges in continental shelf environments would be useful to investigate these issues further.

We show that both τ_e^a and $\tau_{0.8}^a$ decrease with increasing $\mathcal{A}$ and the best fit of our modeled results are given by

$$\tau_e^a(\mathcal{A},\rho) = \begin{cases} (69.6 \times 2.30^{-\log_2\mathcal{A}})\rho^{-6/5} & \text{if } \rho < \rho_e^t; \\ (16.5 \times 1.48^{-\log_2\mathcal{A}})\rho^{-1/2} & \text{if } \rho > \rho_e^t \end{cases} \quad (19)$$

and

$$\tau_{0.8}^a(\mathcal{A},\rho) = \begin{cases} (11.0 \times 2.23^{-\log_2\mathcal{A}})\rho^{-6/5} & \text{if } \rho < \rho_{0.8}^t; \\ (7.3 \times 1.42^{-\log_2\mathcal{A}})\rho^{-1/2} & \text{if } \rho > \rho_{0.8}^t, \end{cases} \quad (20)$$

where ρ_e^t and $\rho_{0.8}^t$ are the transition ranges between the power-law of $\rho^{-6/5}$ and the power-law of $\rho^{-1/2}$ for τ_e^a and $\tau_{0.8}^a$, respectively. We find the transition occurs at ranges where the field covariance or incoherent intensity begins to dominate the total intensity, and the transition range decreases with increasing internal wave energy, as can be seen from Fig. 6. This is mainly due to the severe attenuation induced by multiple forward scattering through internal wave that makes the squared mean field decaying rapidly with range. From Eqs. (19) and (20), we show that the increase in internal wave energy leads to a larger decrease in the acoustic coherence time scales at $\rho < \rho^t$ than that of $\rho > \rho^t$ in continental shelf environments, because the scaling constant, which is a function of $\mathcal{A}$, at $\rho < \rho^t$ is roughly 1.5 greater than that of $\rho > \rho^t$, where ρ^t is the transition range between the power-law of $\rho^{-6/5}$ and the power-law of $\rho^{-1/2}$.

Variations in modeled $\tau_{0.8}^a$ as a function of low ($\mathcal{A} = 1/64$), medium ($\mathcal{A} = 1/4$), and high ($\mathcal{A} = 4$) internal wave energies are found to be of the same order of magnitude as those measured by Yang[18] [Fig. 6(b)]. This consistency gives added confidence to the veracity of our analytical model, which should provide a useful means of estimating or predicting acoustic coherence time scale as a function of internal wave energy in any given continental shelf environment.

IV. CONCLUSION

We have applied an analytical model derived from normal mode theory that includes the accumulated effects of range-dependent multiple forward scattering to estimate the temporal coherence of the acoustic power and field forward propagated through a continental shelf waveguide containing random three-dimensional (3D) internal waves. Knowledge of the acoustic coherence time scale is important in remote sensing applications because it determines (i) the time window within which standard coherent processing, such as matched filtering, beamforming, and synthetic aperture processing, may be conducted, and (ii) the number of *statistically independent* fluctuations in a given measurement period that determines the variance reduction possible by stationary averaging.

The modeled acoustic coherence time is shown to decrease with increasing internal wave energy, to be consistent with measurements from several continental shelf transmission experiments, and to follow a $-1/2$ power-law dependence on range beyond roughly 1 km. The power-law dependencies are consistent with those empirically determined by Yang for low-to mid-frequency signals in various continental shelf environments, and are also consistent with both measured data and ray theory analysis for low- to mid-frequency signals in deep ocean waveguides beyond roughly 10 km range. The model should provide a useful means of estimating or predicting acoustic coherence time scale as a function of internal wave energy in continental shelf waveguides.

[1]R. Urick, *Sound Propagation in the Sea* (Department of Defense, Arlington, VA, 1979), Chap. 11.

[2]R. Dashen, S. Flatte, W. Munk, K. Watson, and F. Zachariasen, *Sound Transmission Through a Fluctuating Ocean* (Cambridge University Press, London, 1979), Chap. 3, pp. 44–61.

[3]P. Porter, R. Spindel, and R. Jaffee, "Acoustic-internal wave interaction at long ranges in the ocean," J. Acoust. Soc. Am. **56**, 1426–1436 (1974).

[4]W. Munk and F. Zachariasen, "Sound propagation through a fluctuating stratified ocean: Theory and observation," J. Acoust. Soc. Am. **59**, 818–838 (1976).

[5]J. L. Spiesberger and P. Worcester, "Fluctuations of resolved acoustic multipaths at long range in the ocean," J. Acoust. Soc. Am. **70**, 565–576 (1981).

[6]P. Porter and R. Spindel, "Low-frequency acoustic fluctuations and internal gravity waves in the ocean," J. Acoust. Soc. Am. **61**, 943–958 (1977).

[7]Y. Desaubies, "On the scattering of sound by internal waves in the ocean," J. Acoust. Soc. Am. **64**, 1460–1469 (1978).

[8]N. C. Makris, "The effect of saturated transmission scintillation on ocean acoustic intensity measurements," J. Acoust. Soc. Am. **100**, 769–783 (1996).

[9]E. Naftali and N. C. Makris, "Necessary conditions for a maximum likelihood estimate to become asymptotically unbiased and attain the Cramer-Rao lower bound. Part I. General approach with an application to time-delay and Doppler shift estimation," J. Acoust. Soc. Am. **110**, 1917–1930 (2001).

[10]R. Dashen, S. Flatte, and S. Reynolds, "Path-integral treatment of acoustic mutual coherence functions for rays in a sound channel," J. Acoust. Soc. Am. **77**, 1716–1722 (1985).

[11]J. L. Spiesberger, F. Tappert, and A. R. Jacobson, "Blind prediction of broadband coherence time at basin scales," J. Acoust. Soc. Am. **114**, 3147–3154 (2003).

[12]T. Chen, P. Ratilal, and N. C. Makris, "Temporal coherence after multiple forward scattering through random three-dimensional inhomogeneities in an ocean waveguide," J. Acoust. Soc. Am. **124**, 2812–2822 (2008).

[13]P. Ratilal and N. C. Makris, "Mean and covariance of the forward field propagated through a stratified ocean waveguide with three-dimensional random inhomogeneities," J. Acoust. Soc. Am. **118**, 3532–3559 (2005).

[14]T. Chen, P. Ratilal, and N. C. Makris, "Mean and variance of the forward field propagated through three-dimensional random internal waves in a continental-shelf waveguide," J. Acoust. Soc. Am. **118**, 3560–3574 (2005).

[15]R. H. Headrick, J. F. Lynch, J. N. Kemp, A. E. Newhall, K. von der Heydt, J. Apel, M. Badiey, C.-S. Chiu, S. Finette, M. Orr, B. Pasewark, A. Turgot, S. Wolf, and D. Tielbuerger, "Acoustic normal mode fluctuation statistics in the 1995 SWARM internal wave scattering experiment," J. Acoust. Soc. Am. **107**, 201–220 (2000).

[16]T. C. Yang, K. Yoo, and M. Siderius, "Internal waves and its effect on signal propagation in the Adventure Bank," in *Proceedings of 8th International Congress on Sound and Vibration*, 3001–3008 (2001).

[17]J. Sellschopp, "High resolution measurements of the ocean fine structure and their relation to sound transmission," in *Proceedings of the Internal Conference on Underwater Acoustic Measurements: Technologies and Results*, edited by J. S. Papadakis and L. Bjorno (Heraklion, Crete, Greece, 2005), pp. 1–8.

[18]T. C. Yang, "Measurements of temporal coherence of sound transmissions through shallow water," J. Acoust. Soc. Am. **120**, 2595–2614 (2006).

[19]H. DeFerrari, J. Lynch, and A. Newhall, "Temporal coherence of mode arrivals," J. Acoust. Soc. Am. **124**, EL104–EL109 (2008).

[20]H. DeFerrari, "Observations of low-frequency temporal and spatial coherence in shallow water," J. Acoust. Soc. Am. **125**, EL45–EL49 (2008).

[21]M. J. Sheehy, "Transmission of 24-kc underwater sound from a deep source," J. Acoust. Soc. Am. **22**, 24–28 (1950).

[22]R. G. Stone and D. Mintzer, "Range dependence of acoustic fluctuations in a randomly inhomogeneous medium," J. Acoust. Soc. Am. **34**, 647–653 (1962).

[23]D. C. Whitmarsh, "Underwater-acoustic-transmission measurements," J. Acoust. Soc. Am. **35**, 2014–2018 (1963).

[24]J. G. Clark and M. Kronengold, "Long-period fluctuations of CW signals in deep and shallow water," J. Acoust. Soc. Am. **56**, 1071–1083 (1974).

[25]F. Dyson, W. Munk, and B. Zetler, "Interpretation of multipath scintillations Eleuthera to Bermuda in terms of internal waves and tides," J. Acoust. Soc. Am. **59**, 1121–1131 (1976).

[26]R. E. Williams and H. F. Battestin, "Time coherence of acoustic signals transmitted over resolved paths in the deep ocean," J. Acoust. Soc. Am. **59**, 312–328 (1976).

[27]I. Dyer, A. B. Baggeroer, P. N. Mikhalevsky, and P. H. Dahl, "Ocean dynamics and acoustic fluctuations in the Fram Strait marginal ice zone," Science **236**, 435–436 (1987).

[28]P. G. Bergmann, "Propagation of radiation in a medium with random inhomogeneities," Phys. Rev. **70**, 486–492 (1946).

[29]L. Liebermann, "The effect of temperature inhomogeneities in the ocean on the propagation of sound," J. Acoust. Soc. Am. **23**, 563–570 (1951).

[30]E. Skudrzyk, "Scattering in an inhomogeneous medium," J. Acoust. Soc. Am. **29**, 50–59 (1957).

[31]L. Rayleigh, "On the transmission of light through an atmosphere containing small particles in suspension, and on the origin of the blue of the sky," London, Edinburgh, Dublin Philos. Mag. J. Sci. **47**, 375–384 (1899).

[32]F. Ingenito, "Scattering from an object in a stratified medium," J. Acoust. Soc. Am. **82**, 2051–2059 (1987).

[33]N. C. Makris and P. Ratilal, "A unified model for reverberation and submerged object scattering in a stratified ocean waveguide," J. Acoust. Soc. Am. **109**, 909–941 (2001).

[34]P. Ratilal and N. C. Makris, "Extinction theorem for object scattering in a stratified medium," J. Acoust. Soc. Am. **110**, 2924–2945 (2001).

[35]H. C. van de Hulst, *Light Scattering by Small Particles* (Dover, New York, 1957), Chaps. 1, 4, and 18.

[36]F. B. Jensen, W. A. Kuperman, M. B. Porter, and H. Schmidt, *Computational Ocean Acoustics*, 2nd ed. (Springer-Verlag, New York, 2011), Chap. 5.

[37]D. Tielburger, S. Finette, and S. Wolf, "Acoustic propagation through an internal wave field in a shallow water waveguide," J. Acoust. Soc. Am. **101**, 789–808 (1997).

[38]T. C. Yang and K. Yoo, "Internal wave spectrum in shallow water: measurement and comparison with the Garret-Munk Model," IEEE J. Ocean. Eng. **24**, 333–345 (1999).

[39]J. R. Apel, M. Badiey, C.-S. Chiu, S. Finette, R. Headrick, J. Kemp, J. F. Lynch, A. Newhall, M. H. Orr, B. H. Pasewark, D. Tielbuerger, A. Turgut, K. von der Heydt, and S. Wolf, "An overview of the 1995 SWARM shallow-water internal wave acoustic scattering experiment," IEEE J. Ocean. Eng. **22**, 465–500 (1997).